Investigation of singlet oxygen generation by photo-active substances when excited by ionizing radiation

Lotte Coffeng

December 6th 2023

TU Delft

Investigation of singlet oxygen generation by photo-active substances when excited by ionizing radiation

By

Lotte K. Coffeng

in partial fulfilment of the requirements for the degree of

Bachelor of Science
in Molecular Science and Technology at the Delft University of Technology,

to be defended publicly on Wednesday December 13, 2023 at 10.30.

Student number:	5188733	
Daily Supervisor:	B. Xu	
Supervisor:	Dr.ir. A.G. Denkova	
Thesis Committee:	Dr.ir. A.G. Denkova	TU Delft
	Dr.ir. Robin de Kruijff	TU Delft

Acknowledgement

I would like to thank my daily supervisor Bing Xu for all her help during this thesis, both on the lab and with writing. I would also like to thank Antonia Denkova for discussing my results with me, brainstorming and all the feedback on my thesis. Lastly I would like to thank Robin de Kruijf for helping me with all my physics related questions and being on my thesis committee.

Abstract

Cancer is often treated by radiation therapy. There are three types of radiation therapy: external beam therapy, brachytherapy and radionuclide therapy. A downside to radiation therapy is its damaging effect on healthy tissue. A different type of treatment is photodynamic therapy. In PDT photo-active substances are being used to generate reactive oxygen species under irradiation. These ROS are a group of radicals which can cause damage to the DNA and in some cases cause necrotic or apoptotic cell death. By combining radiotherapy and PDT, the effectiveness of the treatment can be enhanced.

Among different ROS, singlet oxygen is the most effective in causing DNA damage. As the nanoparticle titaniumdioxide and the photo-active molecule chlorin e6 can generate ROS under ionizing radiation, it is very attractive to look further into how much singlet oxygen they can generate. This report will focus on the singlet oxygen generating abilities of the photo-active substances TiO2 and Ce6 under the irradiation of lutetium-177 and iodine-125. The relative amounts of generated singlet oxygen are measured using a probe called Singlet Oxygen Sensor Green and fluorescence spectroscopy.

The experiments using 177Lu, did not show a lot of promise as a decrease in fluorescence intensity was seen in the radioactive samples. It is possible that 177Lu precipitates despite of its chelation with DTPA and the beta-minus particles might have destroyed the SOSG probe. When comparing the Ce6 samples with the TiO2 samples, the TiO2 samples show much higher intensities. A possible explanation for this result might be the fact that 177Lu destroys both the SOSG and Ce6, whereas TiO2 is not an organic molecules and it thus not destroyed by 177Lu. The intensities of the Ce6 samples was higher than the control group. This suggests there is some positive influence of Ce6 on the generation of singlet oxygen under irradiation of 177Lu.

The experiments using 125I showed promise as the control samples and Ce6 samples showed an increased intensity in the presence of 125I. This suggest that under irradiation of 125I more singlet oxygen is generated than without. The TiO2 samples show inconclusive results and thus no trend can be seen between the exposed and non-exposed samples. This is possible due to some TiO2 particles being present in the eluate.

Nomenclature

Abbreviations

Abbreviation	Definition
Ce6	Chlorin e6
PDT	Photo dynamic treatment
ROS	Reactive oxygen species
TiO2	Titanium dioxide
PS	Photosensitizer
EM	Electromagnetic
177Lu	Lutetium-177
125I	Iodine-125
NP	Nanoparticle

Table 1: Nomenclature

Contents

Introduction

The chance of getting cancer has been increasing in the past three decades. We have now reached the point where almost half the Dutch population, will receive a cancer diagnosis at some point in their life [1].
This shows that more research into improving and finding new ways of treating cancer is imperative. Various currently used treatments are chemotherapy, surgery, radiation therapy, hormone therapy, immunotherapy [2]. In cancer treatment, it is very often chosen to combine certain treatments, to gain better and faster results. A good example is the combination of radiation therapy and chemotherapy. Radiation therapy can be performed by using an external or internal source. In external radiation therapy, a high-energy radiation is delivered precisely to the tumour by beams from outside the body. Internal radiation therapy can be brachytherapy or radionuclide therapy. In brachytherapy a radioactive source is placed inside the patient's body right into the tumour [3]. Often used radioactive sources for this treatment are iridium-192, palladium-103 and iodine-125 [4]. In radionuclide therapy, radioactive substances are administrated to the patient. In these substances a radioisotope is connected to a targeting molecule, which can connect to a specific target protein on the cancer cell. This way tumours can be treated very precisely [5]. Radionuclides like holmium-166, lutetium-177 and rhenium-186 are beta-emitters often used in this treatment [6].

In the past few years, more research is being done on a different type of treatment: photodynamic therapy (PDT) [7]. PDT is already being widely explored for medical imaging and clinical research, and has shown to be an attractive treatment for cancer as well. An advantage of this therapy is that it is an noninvasive medical technique but a disadvantage is the fact that the photo-active substances used in this treatment are harmful to healthy tissue.
In order to perform PDT, a light source having a wavelength that corresponds to the excitation wavelength of the photo-active material is used. This source is used to excite the photo-active substance that is placed inside the body. When the excited photo-active substances come into contact with water and oxygen molecules, cytotoxic reactive oxygen species (ROS), like singlet oxygen are generated. PDT can cause cancer cell death via various cellular mechanisms such as apoptosis, necrosis and provoking immune responses. PDT is considered a good treatment for cancer, since it is considered very effective. PDT does have one major drawback: the weak penetration of the light in the tissue. This limited light penetration is the result of scattering and attenuation of the light after it comes into contact with the tissue. This would mean that the therapy can only be used for superficial or endoscopically accessible tumours [8].

By combining PDT and brachytherapy it might be possible to improve the effectiveness of the treatment when compared to the individual treatments. Previous research in the

Applied Radiation and Isotopes group from TU Delft has shown that ionizing radiation can excite photo-active substances. In this thesis, it will be investigated if the photo-active substances chlorin e6 (Ce6) and titaniumdioxide (TiO2) could be excited by two different types of radiation: low energy gammas (125I) and beta-minus particles (177Lu). A probe called Singlet Oxygen Sensor Green (SOSG) is used for fluorescence spectroscopy, to measure the relative amount of generated singlet oxygen. This probe emits fluorescence when singlet oxygen is present.

Theory

2.1 Electromagnetic Radiation

Electromagnetic radiation (EM radiation) can be ionizing radiation or non-ionizing radiation. The difference lies in the energy of the radiation. Ionizing radiation is capable of removing electrons from materials or breaking bonds within molecules, nonionizing radiation cannot do this as its energy is too low [9]. The difference in energy between the types of radiation is explained by the electromagnetic spectrum. The nonionizing radiation is in the lower side UV-band that corresponds with lower energies, whilst the ionizing radiation is at higher energies in the higher part of the UV-band. Ionizing radiation comes in many forms: X-rays, alpha particles, beta-particles, gamma-rays and positrons. Some examples of nonionizing radiation are: radio waves, UV radiation from the sun,infrared light and radiation in heat lamps [10]. As 177Lu and 125I will be used as radioactive sources in this research, only the decays and emissions that are occur with these isotopes will be discussed.

2.1.1 Radioactivity

The characteristics of an element are defined by the amount of protons in the nucleus of the atom. The number of protons makes up the mass of the atom together with the neutrons. The nucleus of an atom consists of positively charged protons and neutrally charged neutrons. The nucleus is surrounded by a cloud of electrons, which are by definition negatively charged. As positive and negative charges attract each other, the neutrons job is to keep the protons together and away from the electrons [11].

Nuclides are a certain type of atom characterized by the mass of the nucleus. Nuclides where the nucleus has the same number of protons, but a different number of neutrons, are called isotopes. Nuclides have a different mass from the mass of the basic element. A lot of isotopes are stable, which means they do not emit radiation or undergo radioactive decay. An isotope is said to be stable when the nucleus is stable, i.e. the neutrons and protons are in balance with one another. In the case of an unstable atom, the atom will decrease its mass to regain stability, emitting radiation in the process. This is called radioactive decay and the emitted radiation can be an EM wave or particle radiation. After this decay, the parent nuclide is transformed into an atom with different mass and/or amount of electrons called the daughter nuclide [12].

As radioactive decay can cause the emission of EM waves or particle radiation, some examples of particle radiation are alpha decay and beta decay. Alpha particles are quite heavy and consist of 2 protons and 2 neutrons, identical to a helium-4 atom, beta particles can be negatively or positively charged [12]. Examples of EM radiation are the emission of gamma rays and neutrinos, both of which have no mass. The half-life of a nuclide portrays

the rate at which the nuclide decays and is nuclide specific. The nuclide decay always follows the same emission scheme, based on the type of decay [10].

Decay and conversion

Beta-minus decay

When a nuclide has an excess of neutrons, the nucleus will emit an electron from the unstable nucleus, generating beta-minus radiation. Before the emission of the beta-minus particle, it first has to be created, as there are no negatively charged electrons in the nucleus. A beta-minus particle is created when a neutron transforms into an anti-neutrino, beta-minus particle and proton [13]. After the nuclear transformation to a beta-minus particle, which can be seen in Figure 2.1, the beta-minus decay will take place.

$$\mathrm{n} \rightarrow \mathrm{p} + \beta^{-} + \overline{v}$$

Figure 2.1: Neutron nuclear transformation [13]

The beta-minus particles have a continuous spectrum, where alpha particles do not. This is because of the presence of the anti-neutrino in beta-minus decay, which can be seen in Figure 2.2. The anti-neutrino hardly has any mass and has no charge. The maximum value in the spectrum, the endpoint energy, is specific to a nuclide [13]. Beta-minus particles have a greater range than alpha particles but can still be shielded by thin layers of Perspex, water or glass [14]. The beta-minus decay process goes as follows:

$$^{131}_{53}\mathrm{I} \rightarrow ^{131}_{54}\mathrm{Xe} + \beta^{-} + \overline{v}$$

Figure 2.2: Beta-minus decay [13]

Gamma emission

The emission of gamma rays is on itself not a decay process, but rather a decay that accompanies beta or alpha decay. When alpha or beta decay results in an excited state, a gamma photon is emitted to return the particle to the ground state. Gamma rays do not have well-defined ranges like alpha or beta particles, but rather loose a part of their energy per unit distance though matter.
This characteristic makes gamma rays highly penetrable and therefore considerably harmful to organic matter. Heavy shielding is needed for a safe working environment when handling gamma sources. The return of the atom from the excited state to the ground state is usually smaller than 1 nanosecond, but when this is not the case, the excited nucleus is said to be in meta stable or isomeric state, denoted by m [13]. This slower decay process is called isomeric transition and can be seen in Figure 2.3.

$$^{99m}\mathrm{Tc} \rightarrow {}^{99}\mathrm{Tc} + \gamma$$

Figure 2.3: Gamma decay and isomeric transition [13]

Internal conversion
The de-excitation within the nucleus does not always lead to the emission of a gamma-ray. An alternative form is internal conversion, this mode competes with gamma emission. In this process the nucleus is left in an excited state after alfa or beta decay. The excited nucleus emits a gamma ray, which interacts with an atomic electron of the atom and disappears as it transfers its energy to the atomic electron. This excited electron is ejected from its electron shell and the vacancy that it leaves behind is filled by a higher energy electron. Which will emit a X-ray when it jumps to the lower energy shell as its original energy is too high to fill the vacancy [15]. As this electron leaves a vacancy behind, a cascade of electrons will be seen. This cascade can be perceived as either characteristic X-rays or so-called Auger electrons. These two processes are in competition based on the electron configuration of the atom, the atomic number and the electron shells involved. As Auger electrons have a range of only some micrometers to nanometers, the electrons with a relatively low energy are capable of having a much higher linear energy transfer [16].

Radiation sources

In this research, lutetium-177 and iodine-125 were used as radiation source, both are described below.

Lutetium-177
Lutetium-177 is an unstable radioactive isotope of Lutetium. Lutetium is part of the lanthanides, the rare-earth metals. Out of the lantanide series, Lutetium is the last of the series [17]. Lutetium has three oxidation states: 3,2,1. Out of these oxidation states, +3 is the most occurring [18]. Lutetium has 35 isotopes, but for this research only the Lutetium-177 (177Lu) isotope will be used and discussed. The 177Lu isotope is not naturally available on earth, it therefore has to be obtained via radioactive decay of another isotope. 177Lu isotope can be formed via neutron capture of Lu-176 or via beta-minus decay of Ytterbium-177 (Yb-177). The half life of 177Lu is 6.6 days and the isotope will then decay via beta-minus decay to Hafnium-177 (Hf-177). A gamma ray will be emitted during this process with 208 keV or 113 keV [19]. The maximum energy of the decay is 0.497 MeV [17].

Iodine-125
Iodine (I) can be described as a nonmetallic element of the halogen family and has crystalline features. It is the most stable element of the halogens [20]. Currently there are 37 isotopes known of iodine, out of these isotopes 123I, 124I, 125I and 131I are being used in radiation therapy and medicine imaging and 125I is used in this research [21]. The advantage of using 125I in nuclear medicine is the relatively long half-life of 59.7 days,

I-131 for instance, has a half life of only 8 days. Another advantage is the fact that it can occur in nature but can also be manufactured [22]. 125I can be produced from Xenon-124 through various steps of neutron activation. The 125I isotope will decay to an excited state of Tellurium-125 (*Te-125) via electron capture [23]. This excited state will decay immediately by the emission of soft gamma radiation or characteristic x-rays with a maximum energy of 35 keV or Auger electrons are produced [24].

2.1.2 Photon interaction with matter

As photons interact with matter, various effects can occur. These effects are shown in Figure 2.4. The two most important effects are the photoelectric effect and Compton scattering. In the case of Compton scattering, a particle or photon will divert from its original path as it comes into contact with matter. Scattering can either be elastic or inelastic: the interaction with matter is elastic if the kinetic energy remains unchanged after a collision. If the kinetic energy of the photon does change upon collision with matter, it said to be a inelastic interaction. After elastic collision, the photon will continue on a new path. In this new path the photon will cause further ionizations in the matter [25]. Because of this new path, the Compton scattering creates a secondary radiation source within the irradiated material. Both the energy of the photon before interaction with matter and the angle of the scattering, determine the energy of the scattered photon. The probability of Compton effect is directly proportional to the absorber's electron density [26].

In the case of photoelectric effect, all incident photon energy is transferred to an electron, which is then ejected from its orbital. For this effect to take place, energy of the photon must be greater or equal to the ejected electron's binding energy. The atom is ionized after the electron ejection and will be left with a shell electron vacancy in one of its orbitals [26]. As this vacancy cannot stay like this, an electron with a lower binding energy from a lower orbital will fill the vacancy, leaving a new vacancy behind. This new vacancy will then again be filled by an electron with a lower binding energy than the one before. This process results in the emission of so-called Auger electrons or of characteristic x-rays. The photoelectric effect can only occur with high atomic number absorbers [25].

Another important effect of photon interaction with matter is pair production. In this case there is an interaction between the electric field of the nucleus and a photon with an energy higher than 1.02 MeV and in materials with a low atomic number. The photon will disappear after interaction and leave behind an electron and positron. As the positron slows down, it will interact with an electron in the medium and cause annihilation [27]. As a result of annihilation, two annihilation photons are emitted in opposite directions [26]. The photon interactions described before can be seen in Figure 2.5. As 125I emits gamma radiation with around 35 keV, the dominant interaction is the photoelectric effect.

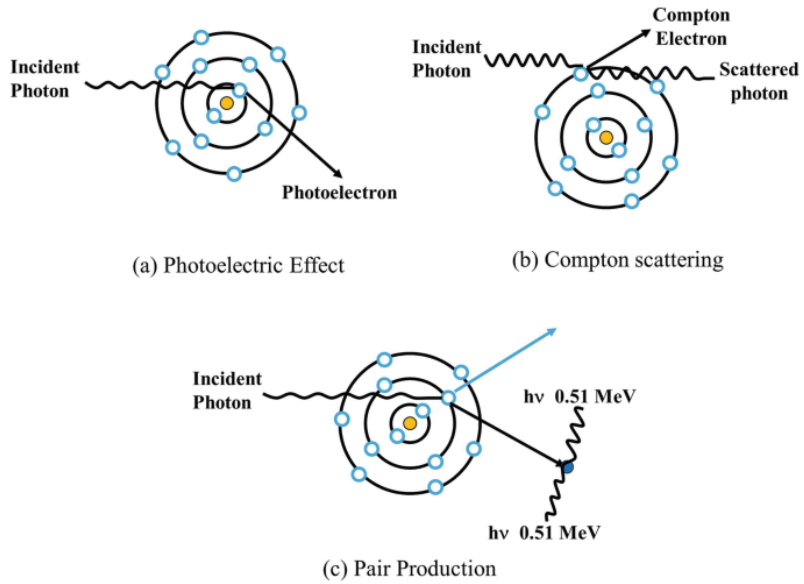

Figure 2.4: Three major interaction of photons [28]

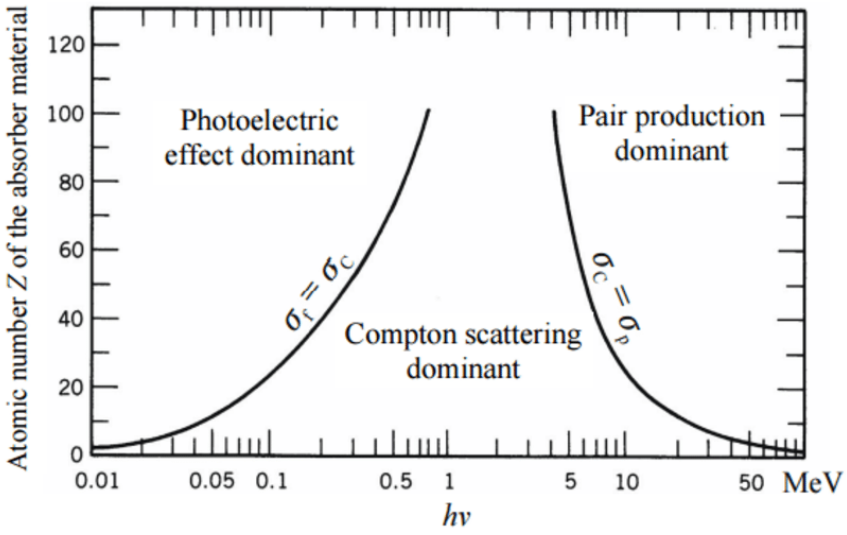

Figure 2.5: Interaction of photons; curtain graph [29]

2.1.3 Beta-minus particle interaction with matter

As beta-minus particles come into contact with matter, various interactions can occur: elastic and inelastic collisions with nuclei, bremsstrahlung or Cerenkov radiation, as can be seen in Figure 2.6.
In the case of elastic interactions, the beta-minus particle will collide with a nucleus and both will change their trajectory after collision. The beta particle will resume its path in a zig-zag pattern though the absorber. The elastic interaction can be electronic, which means that the beta-minus particle collides with an atomic electron and it then scattered, or a nuclear interaction when the beta-minus particle collides with the nucleus of the atom and is then scattered.
Inelastic electronic interaction between the beta-minus particle and an electron in the electron cloud of the atom can result in ionization or excitation. In ionization the incoming beta-minus particle collides with an atomic electron, upon interaction the atomic electron is emitted as it is kicked out of its shell. The resulting atom is now electrically charged. In excitation the beta-minus particle collides with an atomic electron and excites the electron to an electron shell with higher energy [30].
Cerenkov radiation is emitted when charged particles like beta-plus and beta-minus particles move faster than light in the dielectric medium (water in the case of nuclear reactors). The water and oxygen molecules that are in the vicinity of the charged particles, are then excited and emit photons upon relaxation [31].
Even though most interactions between nuclei and electrons are elastic, the electrons can undergo inelastic interactions as well. An example of inelastic nuclear scattering occurs when the negatively charged electron's path is diverted to a new path by the positively charged nucleus of the atom, as the electron is attracted by the nucleus. As the electron loses kinetic energy because of this path deflection, this loss in energy is emitted as EM radiation, i.e. x-rays. The name of this radiation is called bremsstrahlung, which means to "braking radiation"[25]. Although the process of annihilation is shown in Figure 2.6, this interaction can only take place in the presence of beta-plus particles, not beta-minus particles [30].

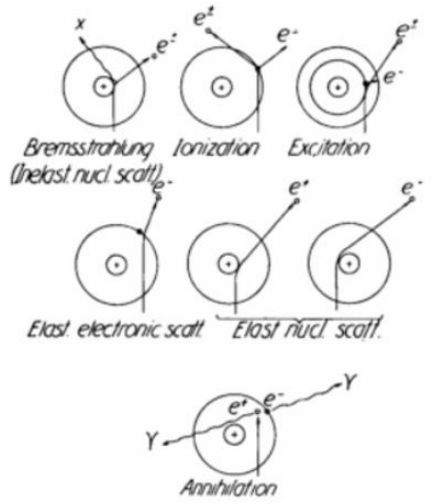

Figure 2.6: Interactions of beta-minus particle with atom [30]

Energy transfer and attenuation

The average amount of energy transferred into the absorber per unit path length, is described by the linear energy transfer, LET for short. The LET is inversely proportional to the kinetic energy (E_k) of the charged particle and proportional to the square of the charge ($\sqrt{Q}$) of the particle (LET $\propto \sqrt{Q}/E_k$) [25]. The LET of a type of radiation shows the impact the radiation can make on a material, which is also known as the local energy deposition density. For instance, high LET radiation, such as protons and alpha particles, transfer their energy over a much smaller range and are in that small range very damaging to, for instance, tissue. The range for low LET radiation can be a lot bigger than for high LET, whilst the damage is more limited [32]. Examples of low LET radiation are gamma rays, x-rays and particle radiation like beta-minus and beta-plus. But for beta particle radiation to be considered low LET, the energy of the radiation has to be low as well. An effect of these high and low LETs in radiotherapy is the fact that in low LETs the energy deposition density might be too low and therefore lead to less effective treatment. The result of using high LETs for radiotherapy can be also harming healthy tissue due to a too large energy deposition energy. Finding the right LET for radiotherapy is therefore crucial. An application of low LET is for instance medical imaging where low LET x-rays or gamma's are often used [25]. As Auger electrons have a range of only some micrometers to nanometers, the electrons with a relatively low energy are capable of having a much higher linear energy transfer. When compared to alpha or beta particles, the Auger electrons' range is significantly shorter in material, this makes them very suitable for targeted radiation therapy [16].

The energy deposition of gamma and x-rays is greatly influenced by attenuation. As a photon beam passes through matter, the intensity of the beam is reduced by attenuation: photons are removed from the photon beam by the matter it passes through. It is the result

of absorption and scattering of primary photons from the beam. The degree of attenuation is determined by factors like the absorber's atomic number and the energy of the photon beam [33]. Attenuation follows the so-called curtain graph, explained in the paragraph before and seen in Figure 2.4. Attenuation is dominated by the photoelectric effect at photon energies lower than 26 keV. As the photoelectric effect is greatly dependant on the atomic number (Z) of the absorber material and the photon energy of the beam, Compton scattering is frequently seen at higher photon energies with low Z absorbers [25].
The attenuation can be described by both the linear attenuation coefficient and the mass attenuation coefficient. While the linear attenuation coefficient is dependant on the density of the material, the mass attenuation coefficient is not. The probability of interaction between gamma and x-rays and a material of a certain thickness, is proportional to the number of atoms in the volume [25]. The resulting intensity of a beam after attenuation can be described by the Lambert-Beer law, Figure 2.7. In this law I_0 is the unattenuated beam intensity and I is the attenuated beam intensity. The linear attenuation coefficient is described by μ (1/cm), t (cm) describes the linear thickness of the absorber and $\mu_m = \mu/\rho$ (cm^2/g) is the mass attenuation coefficient. The density thickness, is described by t_d in g/cm^2 [34].

$$I = I_o e^{-\mu t} = I_o e^{-(\mu/\rho)t_d} = I_o\ e^{-\mu_m t_d}$$

Figure 2.7: Lambert-Beer law for attenuation [34]

2.2 Cancer and Radiotherapy

2.2.1 Progression of cancer in the body

Cancer is a word used for the uncontrolled growth of different types of unhealthy, abnormal cells in the body's tissues. Cancer has various effects, such as loss of organ function and the growth of malignant tumours. The degree of spread (metastasize) of cancer cells to other organs, the bloodstream or lymph system, is dependant on the severity of the decease and the type of cancer [35]. Cancer finds its origin in DNA damage. When there is a change in the basic structure of DNA, like a disruption to a base of DNA, a chemical addition, or a break in one or both chains of DNA strands, one can say there is DNA damage. Problems start to arise when this damaged DNA is then replicated, which will cause mutations in the DNA after more replications. The definition of a DNA mutation is the change in the sequence of the DNA in which a normal base pair is deleted, substituted, added or rearranged. As a result of this mutation, a gene can for instance no longer carry out its function or a gene can be translated into an abnormally functioning protein. Other consequences of DNA mutations can be genomic instability in replicating cells, the activation of oncogenes or the inactivation of tumor suppressor genes. Together all these consequences can lead to cancer. It usually arises when group of mutations confers a

selective advantage which then leads to clonal expansion [36]. "Clonal expansion is the reproduction or multiplication by the division of cells of a population of identical cells, which all originate from the same single precursor" says L. Moreland in *Rheumatology and immunology therapy* [37].

2.2.2 Radiotherapy

In radiotherapy, high-energy X-rays or other types of radiation are used to destroy cancer cells. Radiation therapy consists of a series of treatments given over a set period of time. This type of treatment can be used to treat various types of cancer. It can also be used not mutually exclusive but rather combined with a different type of cancer treatment, such as chemotherapy or surgery. An advantage of radiotherapy is the fact that it can treat cancer locally, this way the amount of healthy tissue damaged can be minimized [7]. Recent changes have been made in the application of external radiotherapy. The radiation dose is increased per treatment and the frequency of treatments is decreased. This results in a higher effectiveness per treatment and the patient has to come to hospital less. Radiotherapy can be performed using various techniques. A choice can for instance be made between using an external or an internal radiation source. In external radiation therapy, radiation will be emitted by a linear accelerator outside the body. There are two types of internal radiation therapy: brachytherapy and radionuclide therapy. In brachytherapy a radioactive source is placed inside the patient's body right into the tumour [3]. Often used radioactive sources for this treatment are iridium-192, palladium-103 and iodine-125 [4]. In radionuclide therapy, radioactive substances are administrated to the patient. In these substances a radioisotope is connected to a targeting molecule, which can connect to a specific target protein on the cancer cell [5].

2.2.3 Radiolysis of water

Radiation therapy mainly relies on the production of reactive oxygen species (ROS), which are generated when water or molecular oxygen (in the tissue) is irradiated [38]. The process of radiolysis of water can be split up into three different stages, as can be seen in Figure 2.8. All these stages have their own time time frames. The first stage of radiolysis is the physical stage, which is the fastest stage at around 1 femtosecond (10^{-15} second).
It takes place right after the initial interaction between the ionizing radiation and water. During this stage, there is a energy deposition, which is followed by a high speed relaxation process. After the relaxation process, the excited water molecules, subexcitation-electrons and ionized water molecules are formed.
During the second stage, the physico-chemical stage, various processes take place like hole diffusion, dissociative relaxation, ion-molecule reactions and thermalization of subexcitation electrons. This stage is a bit slower than the physical stage.
In the last stage, the chemical stage, the species react with one another and with surrounding molecules. In this stage all the final ROS are formed in just 10^{-6} second [39].

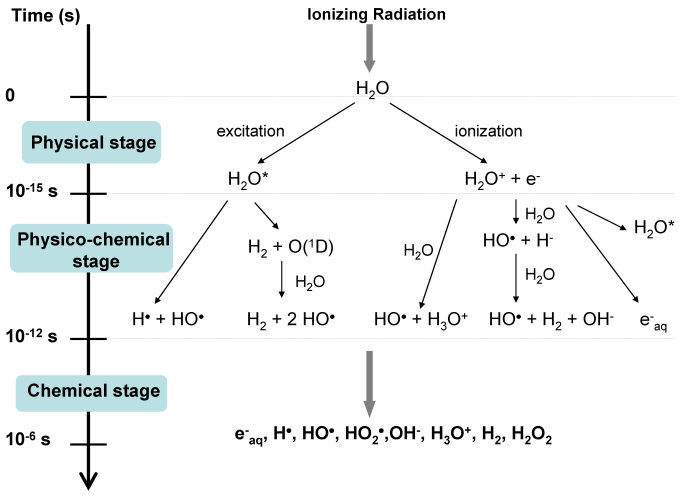

Figure 2.8: Stages of radiolysis of water [39]

2.2.4 Effect of radiotherapy on DNA

In radiotherapy, the target tissue can be treated by causing direct or indirect DNA damage, which can be seen in Figure 2.9. In the case of indirect DNA damage, the radiation beam causes the generation of ROS in the tissue, that will in their turn oxidize lipids and proteins [40]. When looking at DNA damage, the repair system of the cell is first activated, which will stop the cell cycle at certain checkpoints to prevent cycle continuation and to repair the DNA damage. If the DNA repair system of the tumour cell works efficiently enough, the tumour cells will continue to replicate and survive, resulting in radiation resistance. If the repair mechanisms are unable to repair the damages, the repair system will induce apoptosis or programmed cell death to fend off the accumulation of mutations in daughter cells [41].
As a result of these oxidisations, the DNA strands will break. In the case of direct DNA damage, the irradiation of the tissue will directly induce the breaking of DNA strands. Radiotherapy can result in various types of DNA damage, including single-strand breaks (SSBs), abasic sites and double-strand breaks (DSBs) [42].
The linear energy transfer greatly influences the spatial patterns of the DNA damage. When low LET radiation is used, such as X-rays or gamma rays, the damage is uniform and dispersed. With high LET, the damage will be more clustered, scattered along the beam tracks and more discrete. The cell's ability to repair itself, is determined by the number of pathways that work together to repair the separate DNA damages.

The clustered damages caused by high LET radiotherapy, are caused by the pathway of a single radiation track and leave behind two or more independent lesions within one or two DNA helical turns. The DSBs caused by high LET radiation are for the majority clustered DSBs, which are harder to repair than isolated DNA lesions caused by low LET radiation. One can say that by increasing LET of the ionizing radiation, the relative effectiveness of

the radiotherapy increases as well [40].

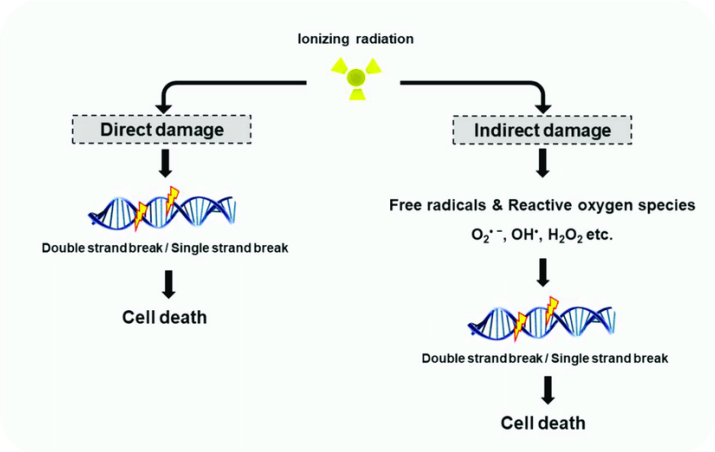

Figure 2.9: Direct and indirect DNA damage by ionizing radiation [43]

2.3 Nanoparticles as photo-active substance

Photodynamic Therapy, PDT, is a cancer treatment based on photo-oxidation reactions of biomolecules. Via these reactions, cell death in tumours is promoted. The following three components are needed for PDT: light, oxygen and a photosensitizer (PS). The PSs are capable of transferring energy from their own triplet state to the oxygen present in the cancerous tissue, which then generates ROS, as can be seen in Figure 2.12. However, some downsides to this type of treatment have come to light during clinical trials. For instance the low solubility of the PS in aqueous media that presents problems like low singlet oxygen generation and aggregation of the PS in the tissue. Another problem is the low accumulation of the PS in the tumour site, which causes healthy tissue to be damaged by the treatment.

A solution to these issues could be introducing nanoparticles (NPs) in PDT. By associating the PSs with NPs, photosensitizing NPs have been formed, which have been proven to be a good enhancement of the treatment. The introduction of NPs can improve the tumour targeting due to better penetration of the tumour, improve the solubility of the PS and enhance the circulation time of the PS [44].

2.3.1 The use of NPs in radiation therapy

To further enhance the efficacy of radiation therapy, the process of radiation sensitization can be implemented. Radiosensitizers are otherwise inert agents, that can improve the effects of radiotherapy when they are irradiated. A big role in the process of sensitization is played by metal based nanoparticles. These high density particles have the ability to

selectively absorb and/or scatter the radiation used in the radiotherapy. As a result, the efficacy of the radiation therapy is enhanced. This means that there is a possibility that the radiation dose can also be further reduced. A requirement for higher cellular damage efficiency, is a high atomic number for the metal nanoparticle. A downside to the radiation sensitization, is the fact that the nanoparticles have to be quite small, otherwise excretion from the body becomes impossible [45]. These two requirements can be difficult to combine. In this research, it is investigated if the nanoparticle TiO2 can enhance the generation of singlet oxygen under irradiation.

2.3.2 Requirements of NPs for cancer treatment

To improve the effect of the nanoparticles in the cancer treatment, the characterisations of the NP have to be investigated. When looking at the size of the NP, it has to be small enough for renal excretion ($\leq$ 10 nm) and also not too small that it will accumulate in healthy tissue [46]. Diffusion into the tumour is still possible at relatively large diameters due to structural defects in tumour cells when compared to healthy cells. Not only the accumulation is determined by the size of the NP, but also the clearance of the NP from the blood circulation and the cytotoxicity. A diameter of around 10 nm is ideal for NPs used in cancer treatment. NPs with this diameter can still enter the tumours while not penetrating too much healthy tissue and it is still possible to excrete the NPs out of the body [47].

2.3.3 Chemical structure of TiO2 and ROS formation

Titanium dioxide (TiO2) is a oxide of titanium, it is an inorganic compound, white of colour and it is insoluble in water [48]. TiO2 is very attractive to use as NP as it is used industrially worldwide and is therefore widely available and also low-cost. When looking at the polymorphism of TiO2, there are various titanium minerals but the ones with the highest titanium content are: anatase, rutile and brookite, which can be seen in Figure 2.10. In all three of these phases, the molecular geometry is octahedral. Within this geometry, three titanium cations share six oxygen anions. Each of these three polymorphisms have their own way of arranging and distorting the geometry and their own shape of octahedral chains. This is the cause for the different properties between the polymorphisms [49].

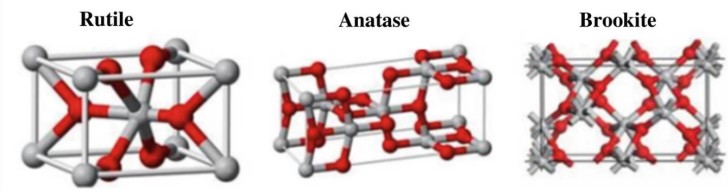

Figure 2.10: Crystal structures of TiO2 [48]

In anatase, the distance between titanium ions is bigger and the distance between the titanium ion and oxygen ion is shorter than in the rutile crystal structure, which explains why

the octahedron chains in anatase are more distorted than in rutile. Whilst each octahedron has eight neighbouring octahedrons in anatase, there are ten neighbouring octahedrons to each octahedron in rutile. This causes a difference in electronic band structures between these crystal structures. The band-gaps for the anatase, rutile and brookite phases are respectively 3.2, 3.02 and 2.96 eV, which makes TiO2 a large band semiconductor.
Since anatase has the biggest band-gap, it is easily explained why this crystal structure has a higher photo-activity than the other structures. As all of these band gap energies are relatively low, rutile and anatase both form gaps in their valence bonds, which explains why they have high oxidation power [48].
When light absorbed by TiO2 has a higher energy than the band gap energy, the electron free conduction band and the by electrons filled valence band will separate as an electron moves from the valence band to the conduction band. This process is called electron-hole pair generation, as a positively charged electron hole is left behind and a 'hole-electron pair' is formed. The highly unstable condition left behind by this process, will react with electrons and molecular oxygen and water molecules [50]. As a result, reactive oxygen species are formed as can be seen in Figure 2.11.
Both the energy band and the surface properties define the photo-catalytic performance of TiO2. For a high performance, a large surface area per mass in the crystal structure is needed, the anatase crystal structure is therefore better suited for photo-catalysis and generation of ROS than rutile [51].

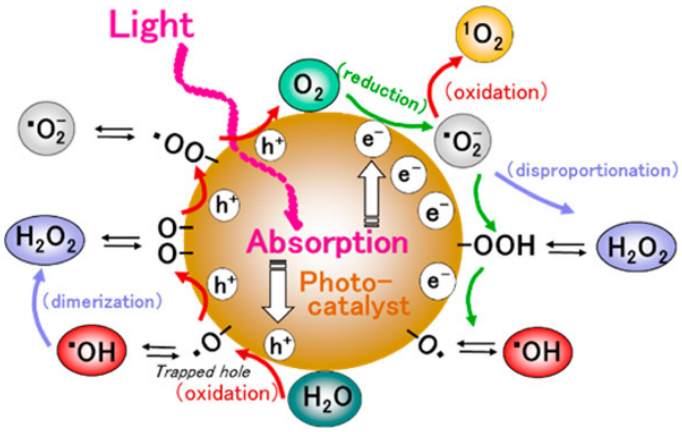

Figure 2.11: ROS formation at TiO2 surface [52]

2.3.4 Chemical structure of Chlorin e6 and ROS formation

Chlorin e6 (Ce6) cannot dissolve in water very well and is a member of the chemical family of chlorins. Chlorins are aromatic compounds. Even though porphyrins are commonly used as photosensitizers, chlorins have shown advantages to porphyrins caused by the two extra hydrogens in chlorins. Due to these two extra hydrogens, the absorption band of Ce6 undergoes a great shift. The absorption band of the chlorin is a lot higher than of porphyrins, resulting in the need for a higher energy laser for electron-hole pair generation. Consequently, deeper tissues can be reached when chlorins are used as photosensitizers [53]. Chlorin e6 has shown photodynamic activity when exposed to light with a wavelength of around 670 nm, which corresponds to a band gap of 1.85 eV [54]. ROS production of at the surface of Chlorin e6 can follow two mechanisms: type I and type II mechanism. In the type I mechanism, the excited chlorin e6 will partake in a electron or hydrogen transfer process, where a radical will be formed which will produce ROS when it comes into contact molecular oxygen or water. The main products of this mechanism are hydroxyl radicals, superoxide anions and hydrogen peroxide. In the type II mechanism, the energy from the excited chlorin e6 is transferred directly to ground state oxygen, which then generates excited state singlet oxygen [55]. The mechanism behind the ROS production can be seen in Figure 2.12.

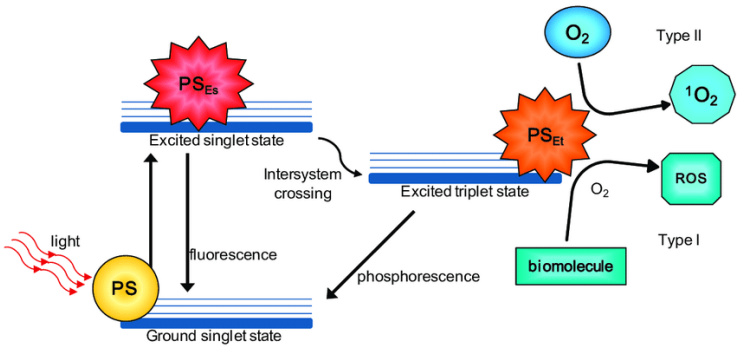

Figure 2.12: Photodynamic therapy mechanism of action [56]

2.4 Experimental analysis

In the experiments, a Singlet Oxygen Sensor Green (SOSG) probe will be used to detect singlet oxygen present in the sample by emitting fluorescence. SOSG has an excitation maximum at 524 nm. Using fluorescence spectrometry, the relative amount of singlet oxygen generated by TiO2 and Ce6 can be determined, based on the maximum intensity around that wavelength. When SOSG is coupled to singlet oxygen, it will emit green fluorescence whilst it emits blue fluorescence without the presence of singlet oxygen [57].

Before the fluorescence spectroscopy, phosphor imaging is done to determine the radiolabeling efficiency of the complexation of Lutetium-177 to DTPA. 177Lu has to be chelated as study done by J. Hu in *The effect of ionizing radiation on singlet oxygen production by Ce6 and TiO2, 2023* has shown that when 177Lu is not chelated, it will precipitate and SOSG will possibly adsorb to the 177Lu particles' surface. Which will result in very little to no fluorescence detection. Iodine-125 does not have to be chelated as it does not precipitate with SOSG.
DTPA is a chelating agent widely used for metal poisoning and removal of isotopes from the body like americium or plutonium. DTPA cannot enter the cell membrane and in between the COO groups in the center of the molecule and the N-site, a center is available for the chelation. In this site up to eight bonds can be formed between the DTPA and metal cations [58]. The chemical structure of DTPA can be seen in Figure 2.13.

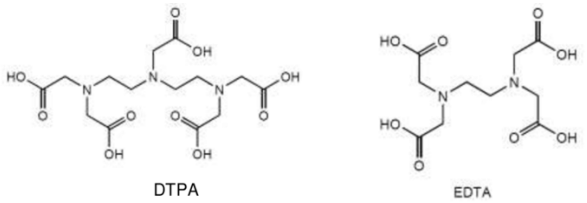

Figure 2.13: Chemical structure DTPA [59]

Phosphorimager/iTLC

Typhoon Variable Mode Imager from Amersham is a variable mode laser scanner. During this research, the storage phosphorimaging mode of the machine was used for iTLC. Latent images produced by ionizing radiation, such as X-rays, beta, and gamma emissions from isotopes can be effectively captured by storage phosphor screens. When stimulated by laser, the storage phosphor screen emits light in direct proportion to the level of radioactivity in the sample. The emitted light is then captured by a photomultiplier tube and recorded during the scanning process. This results in a digital image that allows for precise quantification of even the subtlest variations in signal intensity across a wide dynamic range using the ImageQuant TL software [60].
During this research, the Typhoon Variable Mode Imager was used for determining the chelation efficiency of Lutetium-177 with DTPA in a NaOAC-HOAC buffer. This buffer

was chosen as the pH range of this buffer is ideal for this solution: pH 3.7-5.6. A pH of 5-5.15 was needed for the complexation of 177Lu to DTPA. In TLC, a mobile phase is used to separate the different components in a sample based on how well they dissolve in the mobile phase. The DTPA-Lu complex dissolved better in the mobile phase than the unchelated 177Lu. This way a chelation efficiency could be determined.

Fluorescence spectrometry

The Cary Eclipse Fluorescence Spectrophotometer from Agilent Technologies (MY16240001) is a very effective and powerful way to examine the chemical and physical behaviour of molecules, ideal for trace analysis because of this method's high sensitivity. In fluorescence spectrometry, a sample is irradiated by a beam of light inside the spectrophotometer. The sample is kept at room temperature, since most molecules will be at ground state at that temperature. As a result of the irradiation, some of the molecules in the sample will be elevated to one of their excited states after they absorb part of the light. The molecules, in this case SOSG, will return to their ground state very quickly, releasing the excess energy in the process as fluorescence. This release of energy is detected by the spectrometer and converted from an energy level into a unit called intensity. Both excitation and emission monochromators are present in fluorometers, this makes it possible to measure and combine the wavelength and intensity on respectively the x-axis and y-axis to produce an absorption spectrum [61].

Materials and Methodology

3.1 Materials

3.1.1 List of chemicals

In the list below the other used solutions and salts can be found.

- Acetic acid, purchased from Sigma-Aldrich (CAS 64-19-7)
- Ammonia solution 25%, purchased from Supelco (CAS 1336-21-6)
- Diethylenetriaminepentaacetic acid (DTPA), purchased from Fluka (CAS 67-42-5)
- Hydrochloric acid 11M, purchased from Sigma-Aldrich (CAS 7647-01-0)
- Methanol for HPLC 99%, purchased from Honeywell (CAS 67-56-1)
- Sodium acetate (anhydrous), purchased from Sigma-Aldrich (CAS 127-09-3)

TiO2

The titanium(IV)oxide (CAS 13463-67-7, P-25) was purchased from Degussa. The nanopowder was a mixture of 15% anatase morphology and 85% rutile. The nanopowder had a purity of 99.9% and had an average particle size of 20 nm.

Ce6

The chlorin e6 (CAS 19660-77-6) was purchased from ChemCruz. The Ce6 has to be stored at -20 degrees Celsius and has 96.6% purity.

SOSG

The SOSG probes were stored in vials of 100 µg each and purchased from ThermoFisher.

3.1.2 Radiation sources

Two different radioactive sources were used to perform the experiments: Lutetium-177 and iodine-125.

Lutetium-177

A lutetium-177 source with a original activity of 34 MBq in 0.1 M HCl with a total volume of 50 microliters was used. The source was acquired on October 18 of 2023 from Erasmus MC.

Iodine-125
For the second set of experiments, Iodine-125 was used as radionuclide. A iodine-125 source with a original activity of 200 MBq and volume of 100 microliters was used, which was purchased on September 22 of 2023 from PerkinElmer.

3.1.3 Stock solutions

The TiO2 and Ce6 solutions were prepared by suspending them in MilliQ water. For TiO2, the concentration in the stock solution was 0.5 mg/mL and for the Ce6 stock solution, the concentration was 6 μg/mL. Both stock solutions were sonicated for 20 minutes to create a homogeneous solution. Both stock solutions were covered in aluminium foil and all the samples were kept in black Eppendorf tubes to prevent light degradation of TiO2 and Ce6. Before using the probes, 33 µL of pure methanol was added per vial, to dissolve the SOSG powder. The resulting stock solution had a concentration of 5 mM. For the experiments, the SOSG stock solution of 5 mM was diluted in MilliQ water to get a concentration of 10 μM or 16.5 μM.

3.2 Methodology

Complexation of 177Lu with DTPA and radiolabeling efficiency

A buffer solution was made by mixing 820.3 mg of sodium acetate (NaOAC) with 20 mL of MilliQ and 244.9 μL of acetic acid (HOAC). The pH of this solution was measured, if the pH was higher than 5.15, 2 mL of 0.1 M hydrochloric acid (HCl) was added to lower the pH of the buffer solution.
The DTPA stock solution was made by first making a 1 mM DTPA stock solution in NaOAC/HOAC buffer and then diluted to adjust the molarity to keep the molar ratio 177Lu: DTPA at 1:100. Once the solution was ready, a drop was placed on a TLC paper, 1.5 cm from the bottom of the TLC paper.
A mobile phase for the TLC was made by mixing aqueous ammonia with methanol and MilliQ water in the ratios 0.2:2:4. The chelation efficiency of DTPA with 177Lu in NaOAC/HOAC buffer was determined using iTLC and the ImageQuant phosphor imaging software. This software can determine the intensity in a certain area and by comparing the intensities of the two areas expected to be seen in the TLC: one area that represents the free 177Lu and one that represents the complexed 177Lu, the chelation efficiency of DTPA with 177Lu can be determined.

Singlet oxygen detection

177Lu
Three types of samples were prepared for the singlet oxygen detection experiments: a control group containing 0.6 mL MilliQ water and 0.5 mL of SOSG probe (10 μM or 16.5 μM),

a group containing 0.6 mL of TiO2 solution (0.5 g/L) with 0.5 mL of SOSG probe and a final group of 0.6 mL chlorin e6 (6 μg/mL) with 0.5 mL of SOSG probe. For all three of these groups, six samples were made: three without radioactivity and three with a certain amount of Lu-DTPA solution, corresponding to 0.4 MBq of activity per sample. All samples were prepared in black Eppendorf vials to prevent degradation of the chemicals. The samples were then shaken for 2.5 or 24 hours at 1400 rpm. After shaking, the samples were centrifuged to separate the supernatant from the precipitate in the case of Ce6 and TiO2. Afterwards the samples were transferred into cuvettes by only pipetting the supernatant into the cuvettes. The settings used for the spectrophotometer can be found in Table 3.1. The maximum intensity was taken from the data and this value was usually found around 524 nm.

125I

125I does not have to be chelated to make ROS generation possible. 125I was taken from the stock solution and diluted with MilliQ water, based on the needed volume and activity of the 125I on the day of the experiments. Per sample 10 μL of diluted 125I solution was used and the activity per sample was 0.4 MBq. The same types of samples were made as in the 177Lu experiments. In these experiments the samples were not shaken but just left in the fume hood for 2, 2.5 or 24 hours. The samples were then centrifuged and transferred into the cuvettes for fluorescence spectrometry. The data of these experiments were processed the same way as for the 177Lu samples.

Excitation	504.00 nm
Start	510.00 nm
Stop	600.00 nm
Excitation slit	5.00 nm
Emission slit	5.00 nm

Table 3.1: Settings of Cary Eclipse Fluorescence Spectrophotometer for experiments

Results and Discussion

The generation of singlet oxygen was studied for TiO2 and Ce6 in the presence of radionuclides 177Lu and 125I. The reason behind the choice of these nuclides is the fact that both are already widely used for cancer treatment. The relative amounts of produced singlet oxygen were measured using fluorescence spectroscopy. The results from the fluorescence spectroscopy were given in terms of intensity in the unit a.u., arbitrary unit. The influence of different shaking/incubation times, radionuclides and concentrations of SOSG were investigated. Since SOSG is a relatively unstable molecule, the stability of this probe was also studied.

4.1 177Lu experiments

Two types of experiments were done using 177Lu. First the radiolabeling efficiency of DTPA with 177Lu in NaOAC/HOAC buffer was studied and then the production of singlet oxygen was studied when photo-active materials TiO2 and Ce6 were irradiated by 177Lu. Measurements were done with samples after shaking for 2, 2.5 or 24 hours and centrifuging for 20 minutes at 10.000 rpm and then measuring the supernatant. Three samples of each type were made and the error bars in the graphs show the deviation from the average of the three samples.

4.1.1 Chelation efficiency of 177Lu-DTPA complex

The chelation efficiency of DTPA with 177Lu in NaOAC/HOAC buffer was determined for the first set of samples using iTLC and phosphor imaging. The TLC is expected to show two areas: one area that represents the free 177Lu and one that represents the complexed 177Lu. The free 177Lu area is expected to be seen at the bottom of the TLC, as it does not dissolve very well in the mobile phase and the complexed 177Lu area is expected to be seen higher on the TLC. When comparing the intensities of areas 1 and 2 in Figure 4.1 using the ImageQuant TL software, the chelation efficiency was found to be 94.7%. For the second set of 177Lu samples, the efficiency was found to be 96.2%. Usually the TLC test is followed by a gamma test, in this test a gamma counter is used to measure the activity in 177Lu and is done to make sure the chelation efficiency determined by phosphor imaging is accurate. But as the phospor imaging was already said to be accurate based on previous experiments done with 177Lu in the ARI group, this test was not done. At least an activity of 1 kBq is needed to determine the activity of 177Lu using a gamma counter.

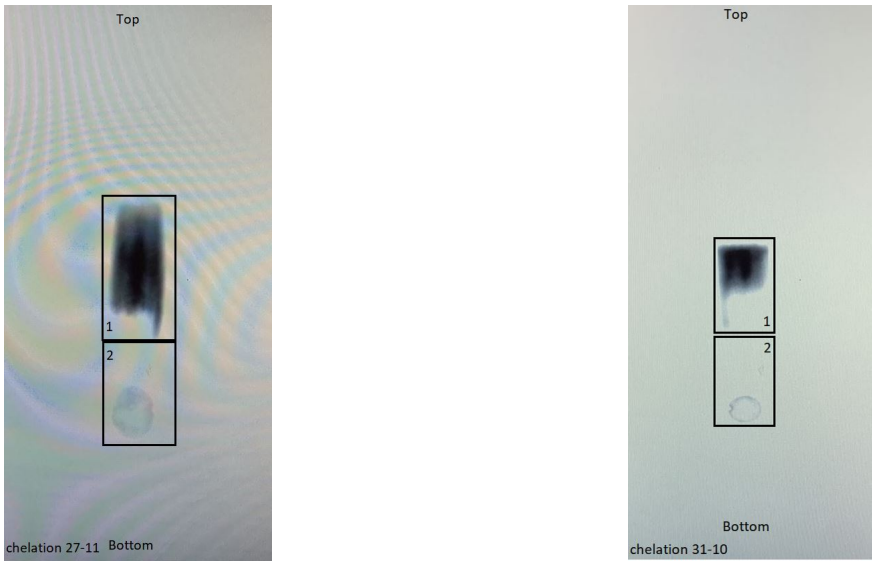

Figure 4.1: Images of TLC strips of first set of 177Lu experiments with 94.7% efficiency (left) and second set of 177Lu experiments with 96.2% efficiency (right)

4.1.2 Singlet oxygen generation

177Lu experiments

In the first set of experiments, SOSG was mixed with 177Lu and either TiO2 or Ce6. The control samples consisted of SOSG in pure water with and without 177Lu. In addition, SOSG was also mixed with TiO2 or Ce6 without 177Lu. Figure 4.2 shows the results for a SOSG concentration of 10 μM and Figure 4.3 for a SOSG concentration of 16.5 μM. Figure 4.2 shows that when only water is mixed with 177Lu, the emission of SOSG remains largely the same irrespective of the incubation time. The small decrease in intensity after longer incubation time can be explained by accidental light exposure in the case of the water and Ce6 samples.
When looking at Figure 4.2, the control group showed a lower intensity in the samples containing activity than the samples without activity. This phenomenon was also seen for the control group in Figure 4.3. This was interesting because one would expect not to see a decrease, as the radioactivity was not expected to decrease the generation of singlet oxygen but rather enhance it.
Samples containing TiO2 showed in Figure 4.2 a much lower SOSG emission with 177Lu irrespective of incubation time. This suggests that there are large uncertainties present which most likely are due to the preparation of the samples. During the centrifuging process and subsequent pipetting of the eluent some TiO2 NPs might come along and they seem to influence the SOSG signal greatly, the precipitate of TiO2 can be seen in Figure 4.4. The decrease in intensity can be due to two reasons. It is possible that 177Lu precipitates despite of its chelation with DTPA. Possibly SOSG absorbs on the precipitates leading to decrease in intensity.

In previous experiments performed by Hu et al it was shown that precipitation does indeed lead to decrease of SOSG signal. The second, very likely reason, could be that the beta minus particle have destroyed the SOSG probe. Recent experiments done by B. Xu of the ARI group have shown that the 177Lu radiation will most likely break SOSG and thus confirm this possibility. The Ce6 results show the same trend suggesting indeed that SOSG might be destroyed. Moreover, intensity in the case of Ce6 decreases slightly as the incubation time increases suggesting indeed that the probe is destroyed. However, the water samples did not show such decrease. It is therefore not entirely clear what the reason for this decrease in intensity is. Figure 4.3 showed a similar result: higher intensity values for the samples without activity than with activity.
When comparing the Ce6 samples with the TiO2 samples, the TiO2 show much higher intensities. Another possible explanation for this result might be the fact that Lutetium-177 destroys both the SOSG and Ce6, whereas TiO2 is not an organic molecules and it thus not destroyed by 177Lu. The intensities of the Ce6 samples was higher than the control group. This suggests there is some positive influence of Ce6 on the generation of singlet oxygen under irradiation of 177Lu. When comparing Figure 4.3 with Figure 4.2, the Ce6 and water samples with the higher SOSG concentration, gave a higher intensity. However, it needs to be mentioned that the intensity of SOSG differs per batch, therefore only interbatch comparison can be made.

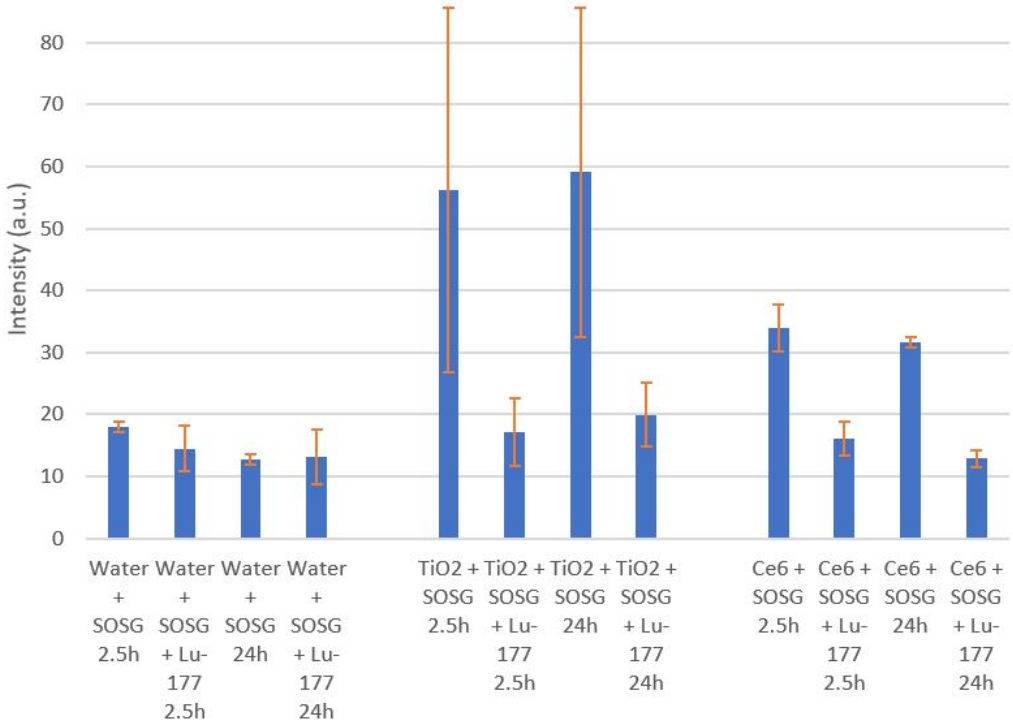

Figure 4.2: Fluorescence intensity of samples containing MilliQ, TiO2 (0.5g/L) or Ce6 (6μg/mL), exposed or non-exposed to 177Lu and shaken for 2.5h or 24h. All samples contained 10μM SOSG

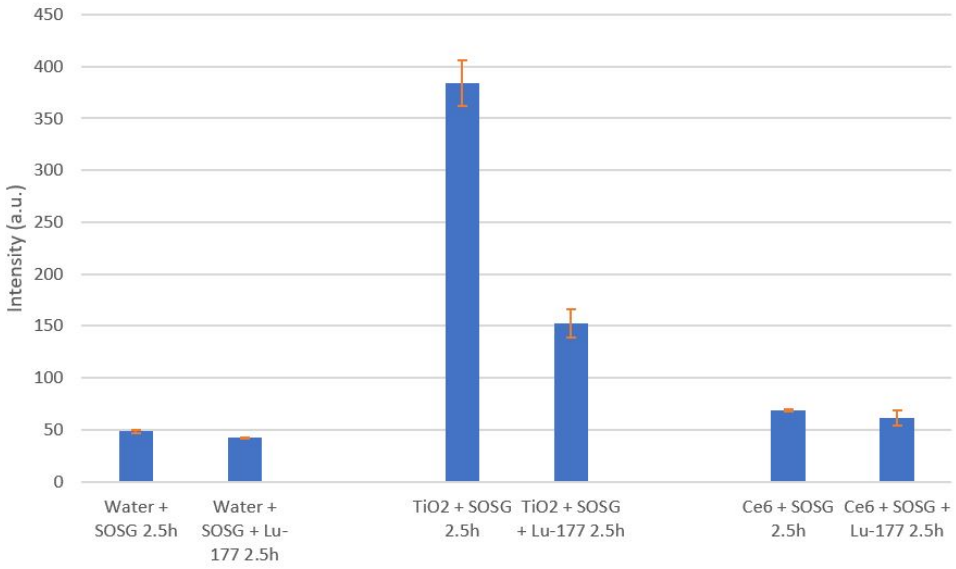

Figure 4.3: Fluorescence intensity of samples containing MilliQ, TiO2 (0.5g/L) or Ce6 (6μg/mL), exposed or non-exposed to 177Lu and shaken for 2.5h. All samples contained 16.5μM SOSG

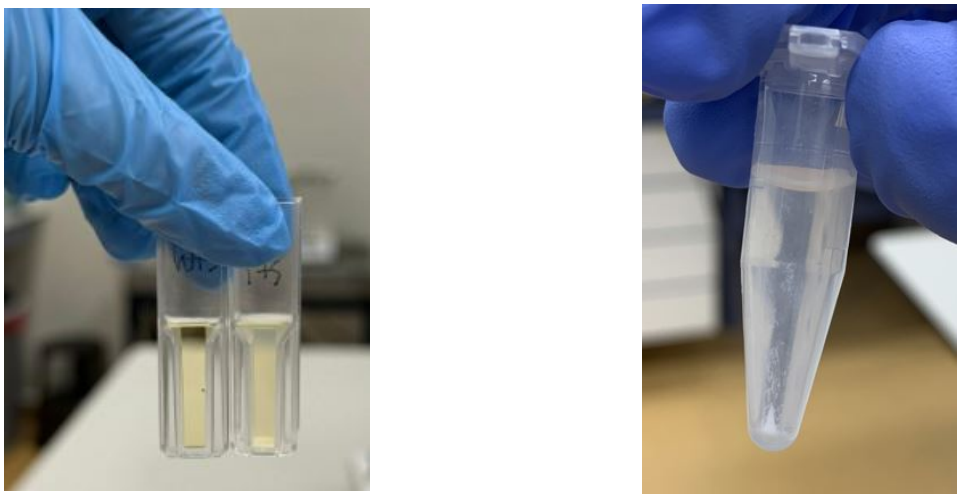

Figure 4.4: Left photo: water sample (left) and TiO2 sample (right) in cuvettes. Right photo: TiO2 precipitate after centrifuging

Based on the results of the experiments with 177Lu shown before, it was chosen to look into the singlet oxygen generation using Ce6 and TiO2 as photo-active substances under irradiation of 125I.

4.2 125I experiments

In these experiments, iodine-125 was used as radiation source and was taken from the stock solution and dissolved in water to get 0.4 MBq of activity per sample. The production of singlet oxygen was measured when using TiO2 or Ce6 as photo-active substances. The samples were incubated after preparation for 2, 2.5 or 24 hours. After incubation, the samples were centrifuged next at 10.000 rpm for 20 minutes and then measuring the supernatant. Three samples of each type were made and the error bars show the deviation from the average of the three samples.

4.2.1 Singlet oxygen generation

The control group showed in Figure 4.5 that the exposed samples resulted in higher intensities than the non-exposed samples. This result was also seen in the control group samples in Figure 4.6. This would suggest that SOSG is slightly activated by 125I in pure water. Longer incubation time did not result in a detectable difference in intensity. When comparing the control samples in Figure 4.5 with Figure 4.6, the higher SOSG concentration samples showed a small increase in intensity. However, it needs to be mentioned that the intensity of SOSG differs per batch, therefore only interbatch comparison can be made.
The Ce6 samples showed in Figure 4.5 and in Figure 4.6 that under exposure to 125I, the intensity increases more than in the case of the water samples. This increase in intensity is not very large and might be influenced by the fact that SOSG itself can act as a photosensitizer, although in only small amounts. More experiments have to be carried out to determine if the difference between the water and Ce6 samples is significant. The non-exposed samples show large uncertainties in Figure 4.5, which might suggest that Ce6 is interacting with the SOSG. When comparing Figure 4.5 with Figure 4.6, the higher SOSG concentration results in higher intensities for the Ce6 samples.

The TiO2 samples show inconclusive results. In Figure 4.5 a small increase in intensity can be seen for the exposed samples, but it is not significant. The results seen in Figure 4.6 are also inconclusive and there is no clear trend. This is possible due to some TiO2 particles being present in the eluate.

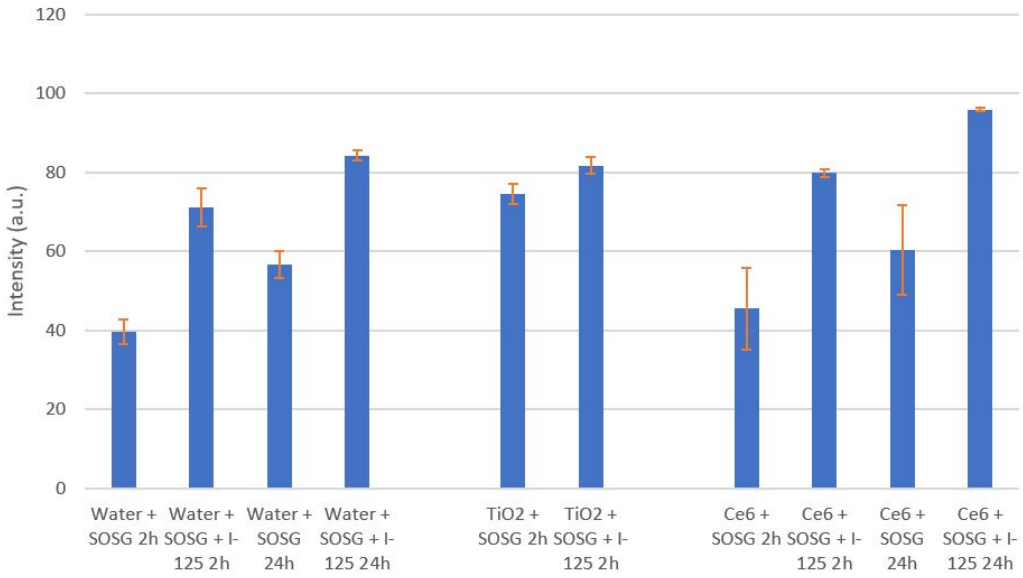

Figure 4.5: Fluorescence intensity of samples containing MilliQ, TiO2 (0.5g/L) or Ce6 (6μg/mL), exposed or non-exposed to 125I and shaken for 2.5h or 24h. All samples contained 10μM SOSG

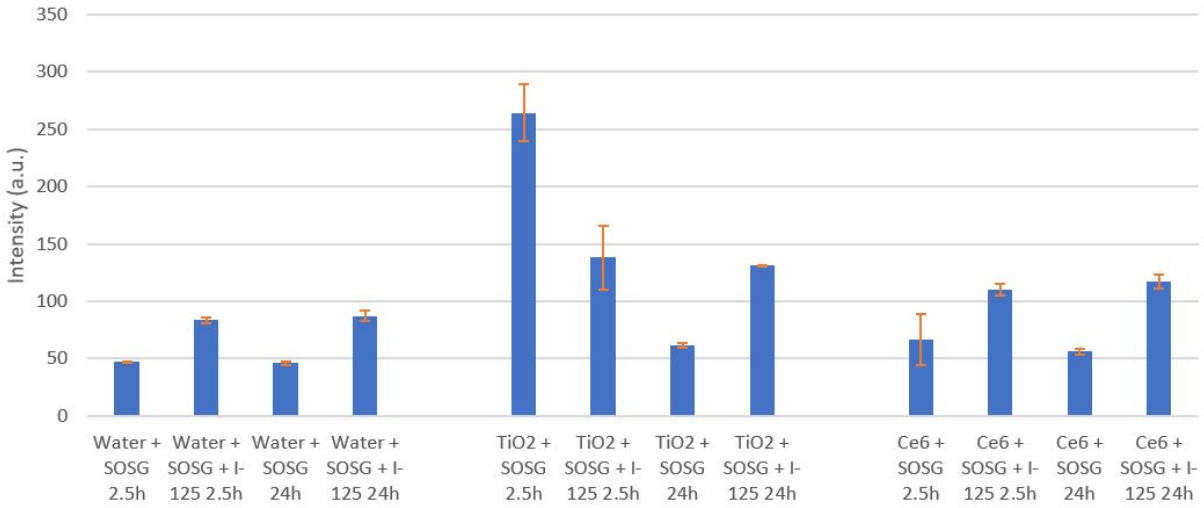

Figure 4.6: Fluorescence intensity of samples containing MilliQ, TiO2 (0.5g/L) or Ce6 (6μg/mL), exposed or non-exposed to 125I and shaken for 2h or 24h. All samples contained 16.5μM SOSG

4.3 Stability of SOSG probe

As Singlet Oxygen Sensor Green is a very sensitive probe which can degrade and fall apart quite easily, it was interesting to look into the stability of this probe. The stability of the probe was tested by measuring the fluorescence of the water samples with and without 125I for a maximum of 96 hours with increments of 24 hours. The control group was used for these experiments as there are no photo-active substances in these samples that can influence the performance and stability of SOSG. The results can be seen in Figure 4.7. The figure showed that for the first two measurements the radioactive samples had a higher intensity than the samples without radioactivity. However, after 48 hours this trend seemed to change.
After 48 hours, the uncertainty in the intensity and the intensity itself started to increase for all samples. This was interesting as a decrease was expected to be seen in both radioactive and non-radioactive samples, as a result of the degradation of SOSG. Based on the results from this experiment, one cannot draw any conclusions on when the integrity of SOSG is compromised. A possible explanations for the increase in intensity and error over time can be light degradation of SOSG or varying SOSG concentrations in the samples.
The degradation of SOSG can be explained by the method used for determining the stability of SOSG. The samples that were measured for each time increment were made on the first day and were transferred from black Eppendorf vials to cuvettes for measuring and then again transferred to the same black Eppendorf vials. This transferring causes the light degradation to increase accumulative over time. Another influence was that even though the samples are mixed after measuring, the SOSG concentration might vary per sample due to pipetting.

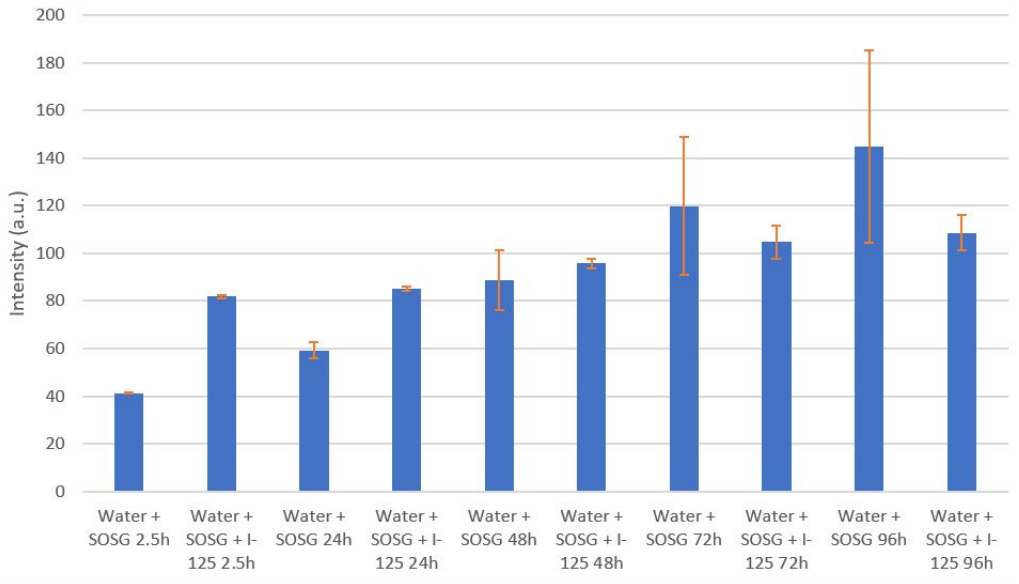

Figure 4.7: Fluorescence intensity for samples containing MilliQ and SOSG (10μM) and exposed or non-exposed the radionuclide 125I for 2.5h, 24h, 48h, 72h, 96h.

Conclusion and Outlook

5.1 Conclusions

The goal of this research was to analyse the ability of photosensitizers such as Ce6 and TiO2 to get activated under ionising radiation of 177Lu and 125I. For the detection of generated singlet oxygen, a SOSG probe was used and its activation was detected using fluorescence spectroscopy. The activity per sample was kept constant at 0.4 MBq for both isotopes while the concentration of SOSG, incubation time and type of radionuclide was varied.

- In order to perform the experiments with 177Lu it was necessary to complex 177Lu with DTPA. Based on the TLC phosphor imaging tests, chelation efficiencies above 90% can be achieved when chelating 177Lu to DTPA in a NaOAC/HOAC buffer.
- The influence of 177Lu on the production of singlet oxygen by TiO2 and Ce6 was investigated revealing that the SOSG signal decreased in the presence of 177Lu. The reason for this decrease is not clear but could be for instance be due to degradation of SOSG by 177Lu and precipitation of 177Lu.
- The 125I experiments showed an increase in intensity when comparing the non-radioactive samples with the radioactive samples in the case of the water and Ce6 samples. This would suggest that 125I has a positive effect on the generation of singlet oxygen in the presence of water and Ce6. This cannot be said for TiO2 as the results for this photo-active material showed to be inconclusive.
- When comparing the two photo-active substances, Ce6 showed slightly more constant increases in intensity under irradiation when compared to TiO2. The results from TiO2 were inconclusive and showed large uncertainties that could be due to precipitation.
- No conclusions can be drawn from the results on the stability of SOSG over time. The results were inconclusive as increasing intensities and errors were observed when irradiation time increased. Possible reasons for these phenomena could be the degradation of the probe and varying SOSG concentration per measurement.

5.2 Outlook

- As the 177Lu showed an unexpected decrease in intensity, possibly due to DTPA being too weak to stay chelated with 177Lu when there are also other compounds in the solution like Ce6, TiO2 or SOSG. It is recommended to look at the chelation efficiency when not only SOSG and the DTPA-Lu complex is present in the sample, but also Ce6 or TiO2. It is also recommended to look into varying the solvent and pH of the DTPA-Lu solution and to perform a gamma-counter test after iTLC to ensure the reliability of the determined chelation efficiency. Based on the results of those experiments, it might be recommended to look into the use of different chelators such as DOTA, if DTPA is proven to be too weak at different pH and in different solvents.

- It is also recommended to look into why exactly the Ce6 samples only show such a small increase when comparing it to the MilliQ samples by for instance doing experiments with similar photo-active molecules. And if that is indeed because 177Lu destroys Ce6 by doing more experiments with Ce6 and other isotopes.

- As the TiO2 samples show inconclusive results, it is recommended to look further into how to decrease the uncertainty in these samples and where the uncertainties can come from. A solution could be increasing the rpm of the centrifuge, this would leave more precipitate at the bottom of the vials. It is also recommended to look into whether or not SOSG sticks to TiO2 and thus TiO2 absorbing the emitted light. A solution could be filtering the TiO2 samples.

- For further research into the longevity of SOSG it is recommended to do more experiments whilst minimizing light exposure and maintaining constant SOSG concentrations. A possible method would be making all the samples for the 5 days of measurements in one time in black Eppendorf vials before the first measurements to ensure constant SOSG concentration. The vials for each day will only be opened on their specific day to decrease light degradation and not be used again.

References

[1] Sept. 2023. URL: https://iknl.nl/nieuws/2023/kansopkanker.

[2] July 2021. URL: https://www.cancerresearchuk.org/about-cancer/treatment.

[3] 2023. URL: https://cancer.gov/about-cancer/treatment.

[4] Michael F. L'Annunziata and Michael F. L'Annunziata. "Radioactivity and Our Well-Being". In: *Radioactivity: Introduction and history, from the quantum to quarks*. 2nd ed. Elsevier, 2016, pp. 1–66.

[5] NCI Staff. *Radiopharmaceuticals emerging as new cancer therapy*. Oct. 2020. URL: https://www.cancer.gov/news-events/cancer-currents-blog/2020/radiopharmaceuticals-cancer-radiation-therapy.

[6] Andrew Hyatt. *Advancing Nuclear Medicine Through Innovation*. 1st ed. National Academies Press, 2007.

[7] Clinic Mayo. *Radiation therapy*. Apr. 2023. URL: https://www.mayoclinic.org/tests-procedures/radiation-therapy/about/pac-20385162.

[8] Dongban Duan, Hui Liu, Yang Xu, et al. "Activating tio2 nanoparticles: Gallium-68 serves as a high-yield photon emitter for Cerenkov-induced photodynamic therapy". In: *ACS Applied Materials amp;amp; Interfaces* 10.6 (2018), pp. 5278–5286. DOI: 10.1021/acsami.7b17902.

[9] Mar. 2020. URL: https://www.nrc.gov/about-nrc/radiation/health-effects/radiation-basics.html.

[10] U.S. Department of Health amp; Human Services. *Radiation studies - CDC: Non-Ionizing Radiation*. Dec. 2015. URL: https://www.cdc.gov/nceh/radiation/nonionizing_radiation.html.

[11] ChemEurope. URL: https://www.chemeurope.com/en/encyclopedia/Radionuclide.html.

[12] Canadiannbsp;Nuclear Safetynbsp;Commission. *Atoms – nuclides and radioisotopes*. Sept. 2019. URL: https://nuclearsafety.gc.ca/eng/resources/radiation/introduction-to-radiation/atoms-nuclides-radioisotopes.cfm.

[13] Gopal B. Saha. *Fundamentals of Nuclear Pharmacy*. 7th ed. Springer, 1992.

[14] Wesley R. Van Pelt Associates. *Beta radiation shielding with lead and plastic: Effect on...: Health physics*. 2007. URL: https://journals.lww.com/health-physics/Abstract/2007/02001/Beta_Radiation_Shielding_with_Lead_and_Plastic_.4.aspx.

[15] Michael F. L'Annunziata and Michael F. L'ANNUNZIATA. "NUCLEAR RADIATION, ITS INTERACTION WITH MATTER AND RADIOISOTOPE DECAY". In: *Handbook of radioactivity analysis*. Academic Press, 2003, pp. 1–121.

[16] B. Q. Lee, T. Kibédi, A. E. Stuchbery, et al. "Atomic radiations in the decay of medical radioisotopes: A physics perspective". In: *Computational and Mathematical Methods in Medicine* (Aug. 2012), pp. 1–14. DOI: 10.1155/2012/651475.

[17] Prof Mark Winter. *Lutetium - 71LU: The essentials*. URL: https://www.webelements.com/lutetium/.

[18] U.S. Department of Energy's NNSA. *PERIODIC TABLE OF ELEMENTS: LANL*. 2021. URL: https://periodic.lanl.gov/71.shtml.

[19] G.P. Thomas. *Lutetium (LU) - discovery, occurrence, production, properties and applications of lutetium*. Apr. 2019. URL: https://www.azom.com/article.aspx?ArticleID=7921.

[20] Karl Christe. *Iodine*. Oct. 2023. URL: https://www.britannica.com/science/iodine.

[21] Tsai-Jung Wu, Hsiao-Yu Chiu, John Yu, et al. "Nanotechnologies for early diagnosis, in situ disease monitoring, and prevention". In: *Nanotechnologies in Preventive and Regenerative Medicine* (2018), pp. 1–92. DOI: 10.1016/b978-0-323-48063-5.00001-0.

[22] PubChem. *Iodine-125*. Mar. 2005. URL: https://pubchem.ncbi.nlm.nih.gov/compound/Iodine-125.

[23] Daiane Souza. *Assessment of the risks associated with iodine-125 handling production ...* Oct. 2015. URL: https://inis.iaea.org/collection/NCLCollectionStore/_Public/47/035/47035623.pdf?r=1&r=1.

[24] Theodore L. Phillips, R. Hoppe, Mack Roach, et al. "Modern Principles of Brachytherapy Physics". In: *Leibel and Phillips Textbook of Radiation Oncology*. Saunders, 2010, pp. 224–244.

[25] Jerrold T. Bushberg. *The Essential Physics of Medical Imaging*. Wolters Kluwer Health/Lippincott Williams amp; Wilkins, 2011.

[26] Stuart C. White and Michael J. Pharoah. "Chapter 1 - Physics". In: *Oral Radiology: Principles and interpretation*. Elsevier, 2014, pp. 1–15.

[27] J. W. Poston. "Dosimetry". In: *Encyclopedia of Physical Science and Technology*. 3rd ed. Academic Press, 2002, pp. 603–650.

[28] Pankaj Tandon, Dibya Prakash, Subhash Chand Kheruka, et al. *Radiation Safety Guide for Nuclear Medicine Professionals*. Springer, 2022.

[29] J. Hyun, P. Piot, and T. Sen. "Optics and Bremsstrahlung estimates for channeling radiation experiments at fast". In: *Optics and bremsstrahlung estimates for channeling radiation experiments at FAST* (Feb. 2018). DOI: 10.2172/1480121.

[30] In: *Acta Radiologica* 51 (1959), pp. 31–39. DOI: 10.3109/00016925909173730.

[31] Chihoon Jo, Heesu Ahn, Ji Hwan Kim, et al. "Cancer therapy by antibody-targeted Cerenkov light and metabolism-selective photosensitization". In: *Journal of Controlled Release* 352 (2022), pp. 25–34. DOI: 10.1016/j.jconrel.2022.10.014.

[32] Maarten Niemantsverdriet, Marc-Jan van Goethem, Reinier Bron, et al. "High and low let radiation differentially induce normal tissue damage signals". In: *International Journal of Radiation Oncology*Biology*Physics* 83.4 (July 2012), pp. 1291–1297. DOI: 10.1016/j.ijrobp.2011.09.057.

[33] M H McKetty. "The AAPM/RSNA physics tutorial for residents. X-ray attenuation." In: *RadioGraphics* 18.1 (Feb. 1998), pp. 151–163. DOI: 10.1148/radiographics.18.1.9460114.

[34] Ripan Biswas, Hossain Sahadath, Abdus Sattar Mollah, et al. "Calculation of gamma-ray attenuation parameters for locally developed shielding material: Polyboron". In: *Journal of Radiation Research and Applied Sciences* 9.1 (Jan. 2016), pp. 26–34. DOI: 10.1016/j.jrras.2015.08.005.

[35] Janet M. Torpy, Cassio Lynm, and Richard M. Glass. "Cancer: The basics". In: *JAMA* 304.14 (Oct. 2010), p. 1628. DOI: 10.1001/jama.304.14.1628.

[36] Clark Chen. *New research directions in DNA repair*. InTech, 2013.

[37] Larry W. Moreland. "Clonal expansion". In: *Rheumatology and immunology therapy A to Z essentials; with 33 tables*. Springer, 2004, pp. 226–227.

[38] Markus F Renschler. "The emerging role of reactive oxygen species in cancer therapy". In: *European Journal of Cancer* 40.13 (Sept. 2004), pp. 1934–1940. DOI: 10.1016/j.ejca.2004.02.031.

[39] Sophie Le Caër. "Water radiolysis: Influence of oxide surfaces on H2 production under ionizing radiation". In: *Water* 3.1 (2011), pp. 235–253. DOI: 10.3390/w3010235.

[40] Sharda Kumari, Shibani Mukherjee, Debapriya Sinha, et al. "Immunomodulatory effects of radiotherapy". In: *International Journal of Molecular Sciences* 21.21 (Oct. 2020). DOI: 10.3390/ijms21218151.

[41] Gissela Borrego-Soto, Rocío Ortiz-López, and Augusto Rojas-Martínez. "Ionizing radiation-induced DNA injury and damage detection in patients with breast cancer". In: *Genetics and Molecular Biology* 38.4 (Oct. 2015), pp. 420–432. DOI: 10.1590/s1415-475738420150019.

[42] Rajeshwar P. Sinha. "Molecular mechanisms of ultraviolet radiation-induced DNA damage and repair". In: *Journal of Nucleic Acids* 2010 (Dec. 2010), pp. 1–32. DOI: 10.4061/2010/592980.

[43] Eliza Rocha Gomes and Marina Santiago Franco. "Combining nanocarrier-assisted delivery of molecules and radiotherapy". In: *Pharmaceutics* 14.1 (Jan. 2022), p. 105. DOI: 10.3390/pharmaceutics14010105.

[44] Dayane B. Tada and Mauricio S. Baptista. "Photosensitizing nanoparticles and the modulation of Ros Generation". In: *Frontiers in Chemistry* 3 (May 2015). DOI: 10.3389/fchem.2015.00033.

[45] Deep Kwatra, Anand Venugopal, and Shrikant Anant. "Nanoparticles in radiation therapy: A summary of various approaches to enhance radiosensitization in cancer". In: *Translational Cancer Research* 2 (Aug. 2013), pp. 330–342. DOI: 10.3978/j.issn.2218-676X.2013.08.06.

[46] Chung Hang Choi, Jonathan E. Zuckerman, Paul Webster, et al. "Targeting kidney mesangium by nanoparticles of defined size". In: *Proceedings of the National Academy of Sciences* 108.16 (2011), pp. 6656–6661. DOI: 10.1073/pnas.1103573108.

[47] Randa Zein, Wissam Sharrouf, and Kim Selting. "Physical properties of nanoparticles that result in improved cancer targeting". In: *Journal of Oncology* 2020 (2020), pp. 1–16. DOI: 10.1155/2020/5194780.

[48] Şana Sungur. "Titanium dioxide nanoparticles". In: *Handbook of Nanomaterials and Nanocomposites for Energy and Environmental Applications* (2021), pp. 713–730. DOI: 10.1007/978-3-030-36268-3_9.

[49] Ulrike Diebold. "The surface science of titanium dioxide". In: *Surface Science Reports* 48.5–8 (2003), pp. 53–229. DOI: 10.1016/s0167-5729(02)00100-0.

[50] Janusz Bogdan, Agnieszka Jackowska-Tracz, Joanna Zarzyńska, et al. "Chances and limitations of nanosized titanium dioxide practical application in view of its physicochemical properties". In: *Nanoscale Research Letters* 10.1 (2015). DOI: 10.1186/s11671-015-0753-2.

[51] Ali Reza Khataee and G. Ali Mansoori. *Nanostructured titanium dioxide materials properties, preparation and applications*. World Scientific Publishing, 2012.

[52] Yoshio Nosaka and Atsuko Y. Nosaka. "Generation and detection of reactive oxygen species in photocatalysis". In: *Chemical Reviews* 117.17 (Aug. 2017), pp. 11302–11336. DOI: 10.1021/acs.chemrev.7b00161.

[53] Arshadul Hak, Mohammad Sadik Ali, Sri Amruthaa Sankaranarayanan, et al. "Chlorin E6: A promising photosensitizer in photo-based cancer nanomedicine". In: *ACS Applied Bio Materials* 6.2 (2023), pp. 349–364. DOI: 10.1021/acsabm.2c00891.

[54] Lyubov V. Kostryukova, Vladimir N. Prozorovskiy, Natalya V. Medvedeva, et al. "Comparison of a new nanoform of the photosensitizer chlorin E6, based on plant phospholipids, with its free form". In: *FEBS Open Bio* 8.2 (2018), pp. 201–210. DOI: 10.1002/2211-5463.12359.

[55] Alessia Marconi, Edoardo Jun Mattioli, Filippo Ingargiola, et al. "Dissecting the interactions between chlorin E6 and human serum albumin". In: *Molecules* 28.5 (Mar. 2023), p. 2348. DOI: 10.3390/molecules28052348.

[56] Giovana Calixto, Jéssica Bernegossi, Laura de Freitas, et al. "Nanotechnology-based drug delivery systems for photodynamic therapy of cancer: A Review". In: *Molecules* 21.3 (Feb. 2016), pp. 21–342. DOI: 10.3390/molecules21030342.

[57] C. Flors. *Singlet oxygen sensor green - special packaging*. URL: https://www.thermofisher.com/order/catalog/product/S36002.

[58] Aug. 2022. URL: https://www.bioblast.at/index.php/DTPA.

[59] Martin A. Hubbe, Jeremy R. Metts, Daphne Hermosilla, et al. "Wastewater treatment and reclamation: A review of Pulp and paper industry practices and opportunities". In: *BioResources* 11.3 (Aug. 2016), pp. 7953–8091. DOI: 10.15376/biores.11.3.hubbe.

[60] Josh Luffman. *FLA7000IP Typhoon Storage phosphorimager*. Sept. 2018. URL: https://lab.vanderbilt.edu/cdb-core-lab/fla7000ip-typhoon-storage-phosphorimager/.

[61] Toyoichi Tanaka and H. Igataki. "Fluorescence spectroscopy". In: *Experimental methods in polymer science: Modern methods in polymer research and technology*. Academic Press, 2012, pp. 155–157.